THE PUBLISHING HOUSE
OF THE ROMANIAN ACADEMY

PROCEEDINGS OF THE ROMANIAN ACADEMY, Series A,
Volume 22, Number 1/2021, pp. 43–52

ANT LION OPTIMIZER: A NOVEL STRATEGY FOR GLOBAL ENGINEERING OPTIMIZATION OF STRESS IN INFINITE PERFORATED COMPOSITE PLATES SUBJECT TO HEAT FLUX

Mohammad JAFARI[1], Mohammad Hossein Bayati CHALESHTARI[2], Eduard-Marius CRACIUN[3]

[1] Shahrood University of Technology, Faculty of Mechanical and Mechatronics Engineering, Shahrood, Iran
[2] Iran University of Science and Technology, School of Mechanical Engineering, Narmak, Tehran, Iran
[3] "Ovidius" University of Constanta, Faculty of Mechanical, Industrial and Maritime Engineering, Romania

Corresponding author: E.-M. Craciun, E-mail: mcraciun@univ-ovidius.ro

Abstract. The presence of geometric discontinuities within composite plates subject to a constant heat flux causes severe thermal stress. This study tries to examine the optimum design of infinite perforated plates subjected to the constant heat flux. The influential factors affecting the normalized stress around a quasi-square hole are fiber angle for the composite material, angle of flux, bluntness, and the hole rotation angle. Using Ant Lion Optimizer (ALO), the optimal values of the aforementioned parameters are calculated. By applying the complex variable approach, the composite infinite plate with a circular hole is mapped to the plate with a quasi-square hole. The perforated plate is under heat flux and thermal insulated state on the hole's edge is considered as thermal boundary condition. The results show that by selecting the correct values of the mentioned parameters, the lowest normalized stress around the hole can be achieved which leads to the enhancement of the load bearing capacity of the perforated plate.

Key words: infinite composite plate, quasi-square hole, complex variable method, ant lion optimizer, uniform heat flux.

1. INTRODUCTION

Perforated plates are seen in numerous industrial applications. When these plates are subjected to heat flux, the severe stress concentration around the geometrical discontinuities is created. Therefore, given the wide use of composite materials and their relevant complex feedback to thermal loads, the influential factors leading to a decrease in stress concentration in various structures must be cautiously considered.

There are a few studies on the thermal stress analysis of perforated composite plates [1–6]. Lately, an original bio-inspired algorithm named the Ant Lion Optimizer (ALO) was suggested by Mirjalili [7] that exhibits behavior similar to that of ant lions when hunting ants in nature. Although the effectiveness of different optimization methods on stress analysis of perforated plates has been demonstrated in various papers [8, 9]. The current study calculates the optimal values of influential parameters on thermal stress distribution around a quasi-square hole in composite plates using ALO. Bluntness parameter, fiber angle, and hole orientation are considered as design variables. In this study, it is attempted to present optimal values for the aforementioned parameters for the plate with different quasi square holes undergoing constant heat flux for the purpose of achieving minimum normalized thermal stress.

2. PROBLEM DEFINITION

As shown in Fig. 1, an infinite composite plate containing a quasi-square hole in its center under a remote constant heat flux q with angle δ relative to the x-axis is considered. γ represents the fiber angle. The quasi-square hole edge is considered as insulated. The hole rotation angle that represents its orientation in relation to the horizontal axis is shown by β.

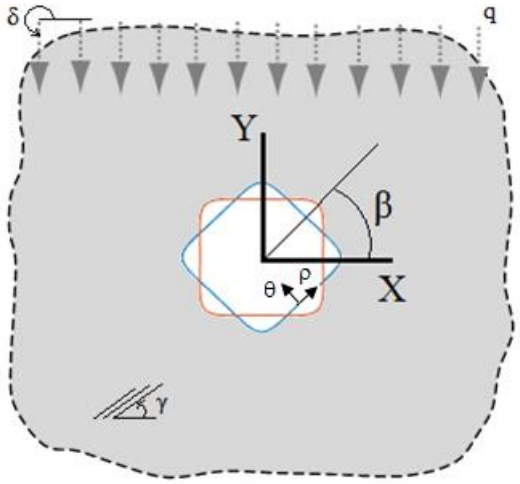

Fig. 1 – Infinite composite plate a containing quasi-square hole under uniform heat flux.

3. THEORETICAL FORMULATION

By introducing the Airy stress functions $F(x,y)$ and $\psi(x,y)$, the compatibility equations of anisotropic materials in regard to the stress functions are provided as follows [10]:

$$\begin{aligned} L_4 F + L_3 \psi &= -\alpha_2 \frac{\partial^2 T}{\partial x^2} + \alpha_6 \frac{\partial^2 T}{\partial x \partial y} - \alpha_1 \frac{\partial^2 T}{\partial y^2} \\ L_3 F + L_2 \psi &= \alpha_4 \frac{\partial T}{\partial x} - \alpha_5 \frac{\partial T}{\partial y} \end{aligned} \tag{1}$$

where α_i are the thermal expansion coefficients, and T is the temperature gradient. Also, L_2, L_3 and L_4, in relation (2), are order 2, 3 and 4 differential operators, as follows [10]:

$$\begin{aligned} L_2(\mu) &= S_{55}\mu^2 - 2S_{45}\mu + S_{44} \\ L_3(\mu) &= S_{15}\mu^3 - (S_{14} - S_{56})\mu^2 + (S_{25} + S_{46})\mu - S_{24} \\ L_4(\mu) &= S_{11}\mu^4 - 2S_{16}\mu^3 + (2S_{12} + S_{66})\mu^2 - 2S_{26}\mu + S_{22} \end{aligned} \tag{2}$$

where $\bar{S}_{ij}$ are the orthotropic compliance matrix components where μ_k is the solution of the characteristic Eq. (3):

$$L_4(\mu)L_2(\mu) - L_3^2(\mu) = 0\,. \tag{3}$$

The established terms for the stress functions F and ψ are dependent on μ_k, the roots of the above characteristic equation. The stress components are acquired in regard to stress function shown below [10]:

$$\begin{aligned} \sigma_x &= \mathrm{Re}\left\{\mu_1^2\phi_1'(Z_1) + \mu_2^2\phi_2'(Z_2) + \mu_3^2\lambda_3\phi_3'(Z_3)\right\} + 2\,\mathrm{Re}\left(\eta_1\mu_t^2\phi_t'\right) \\ \sigma_y &= \mathrm{Re}\left\{\phi_1'(Z_1) + \phi_2'(Z_2) + \lambda_3\phi_3'(Z_3)\right\} + 2\,\mathrm{Re}\left(\eta_1\phi_t'\right) \\ \tau_{xy} &= -2\,\mathrm{Re}\left\{\mu_1\phi_1'(Z_1) + \mu_2\phi_2'(Z_2) + \mu_3\lambda_3\phi_3'(Z_3)\right\} - 2\,\mathrm{Re}\left(\eta_1\mu_t\phi_t'\right). \end{aligned} \tag{4}$$

The resulting stress functions are determined as equation (5) in terms of complex variable $Z_k = x + \mu_k y$ for $k = 1,2,3,t$:

$$\phi_k(Z_k) = F_k'(Z_k)\,, \qquad k = 1,2,3,t\,. \tag{5}$$

In relation 4, μ_t is the root of the characteristic Eq. (6):

$$K_{22}\mu_t^2 + 2K_{12}\mu_t + K_{11} = 0. \tag{6}$$

In the relation above, K_{ij} is anisotropic thermal conductivity matrix. Since the thermal conductivity matrix is positive definite and invertible $K_{11}K_{22} > K_{12}^2$, thus, the characteristic Eq. (6) has two conjugate roots, which the roots with positive imaginary part are taken into account. Using such method, the problem is restricted to the calculation of stress function ϕ_1, ϕ_2, ϕ_3 and ϕ_t that satisfy the mechanical and thermal boundary condition around the hole [9]. In order to expand the analytical solution related to a circular hole to a quasi-square hole as well as simplifying the employment of the Cauchy integral formula, the outside infinite region of the quasi-square hole is mapped to the outside of a unit circle. The implemented mapping function for this study is presented below:

$$Z_k = \omega(\zeta) = x + \mu_k y, \quad k = 1,2,3,t. \tag{7}$$

Such that x and y represent the points' coordinates within the plate with thesquare hole and may be provided in regard to θ shown below [10]:

$$\begin{aligned} x &= (\cos\theta + \omega\cos(3\theta)) \\ y &= (c\sin\theta - \omega\sin(3\theta)), \end{aligned} \tag{8}$$

μ_k being the roots of thecharacteristic equation of anisotropic materials metioned previously.

The parameter ζ from the mapped plane is determined as follows:

$$\zeta = \rho e^{i\theta} = \rho(\cos\theta + i\sin\theta). \tag{9}$$

Concerning the unit circle ρ =1. For the relationship above, c regulates the hole elongation in the y-direction and ω represents the hole corners' curvature. Figure 2 depicts the impact of the ω parameter concerning the curvature of the hole corners.

Fig. 2 – Effect of the parameter ω on the curvature of the holes.

4. OPTIMIZATION PROCESS

The effective parameters of each algorithm, namely the ALO, Particle Swarm Optimization (PSO) and Genetic Algorithms (GA) affect the premature convergence and convergence rate, leading to an optimal solution. Upon changing and optimizing the parameters, an optimally performing algorithm is obtained. It is noteworthy that the outcomes of the three optimization algorithms are provided for the glass/epoxy wet plate with quasi-square hole.

4.1. Ant Lion Optimizer algorithm

The ALO algorithm imitates the activity exhibited by ant lions when hunting i.e. interactions among the predator (ant lions) and prey (ant). Similar to other insects, ants detect food easily using stochastic behavior. Such behavior is mathematically presented by the equations as follows:

$$X(t) = \left[0, cumsum(2r(t_1) - 1), cumsum(2r(t_2) - 1), \ldots, cumsum(2r(t_n) - 1)\right]. \tag{10}$$

Such that *cumsum* derives the cumulative sum, *n* is the maximal iteration number, *t* exhibits the stage of random walk and *r*(*t*) is a stochastic function calculated as Eq. (11):

$$r(t)=\begin{cases}1 & \text{if} \quad rand>0.5\\ 0 & \text{if} \quad rand\le 0.5\end{cases}. \tag{11}$$

Such that *t* exhibits the stage of random walk and *rand* is a random number produced with homogenous distribution in the range of [0, 1]. The ants' positions are preserved in a M_{Ant} matrix:

$$M_{Ant}=\begin{bmatrix} A_{1,1} & A_{1,2} & \cdots & A_{1,d}\\ A_{2,1} & A_{2,2} & \cdots & A_{2,d}\\ \vdots & \vdots & \ddots & \vdots\\ A_{n,1} & A_{n,2} & \cdots & A_{n,d}\end{bmatrix} \tag{12}$$

where $A_{i,j}$, exhibits the value of the j^{th} variable of i^{th} ant, *n* denotes the quantity of ants, and *d* is the number of variables. cost function of every ant is preserved in the matrix M_{OA}.

Such that f is the cost function. In Eq. (13), $M_{Antlion}$ is the matrix for preserving the position of every ant lion, $AL_{i,j}$ exhibits the *j*-th dimension's value of *i*-th ant lion [4]:

$$M_{OA}=\begin{bmatrix} f([A_{1,1},A_{1,2},\ldots,A_{1,\mathrm{d}}])\\ f([A_{2,1},A_{2,2},\ldots,A_{2,\mathrm{d}}])\\ \vdots\\ f([A_{n,1},A_{n,2},\ldots,A_{n,\mathrm{d}}])\end{bmatrix} \qquad M_{Antlion}=\begin{bmatrix} AL_{1,1} & AL_{1,2} & \cdots & AL_{1,n}\\ AL_{2,1} & AL_{2,2} & \cdots & AL_{2,\mathrm{d}}\\ \vdots & \vdots & \ddots & \vdots\\ AL_{n,1} & AL_{n,2} & \cdots & AL_{n,\mathrm{d}}\end{bmatrix} \tag{13}$$

Comparatively, fitness function of every ant lion is preserved within the matrix M_{OAL}:

$$M_{OAL}=\begin{bmatrix} f([AL_{1,1},AL_{1,2},\ldots,AL_{1,d}])\\ f([AL_{2,1},AL_{2,2},\ldots,AL_{2,d}])\\ \vdots\\ f([AL_{n,1},AL_{n,2},\ldots,AL_{n,d}])\end{bmatrix} \tag{14}$$

The following section presents the five underlying phases concerning the hunting approach of ant lions. In the first step, the position of ants is updated *b* to *a* random walk search Eq. (10) Then, normalization is conducted using Eq. (15) to ensure that every position of the ants is within the search space boundary. Where the a_i, b_i are the minimal and maximal random walks pertinent to i^{th} variable, c_t^i and respectivell d_t^i are indicating the minimal and maximal i^{th} variables at t^{th} iteration, respectively. Moreover, in second step, of ants trapping mathematical modelling for the pits of ant lions provided by the Eq. (15):

$$\begin{aligned} X_i^t &= \frac{(X_i^t-a_i)\times(b_i-c_i^t)}{(\mathrm{d}_i^t-a_i)}+c_i\\ c_i^t &= Antlion_j^t+c^t\\ d_i^t &= Antlion_j^t+d^t. \end{aligned} \tag{15}$$

Third step shows the building traps. For the purpose of modelling the hunting competency of ant lions, a roulette wheel is implemented. Figure 3 shows that ants are considered trapped in just one chosen ant lion. The ALO algorithm must employ a roulette wheel operator to choose ant lions on the basis of fitness levels amidst optimization. Such mechanism provides significant opportunity to the fit ant lions to hunt ants.

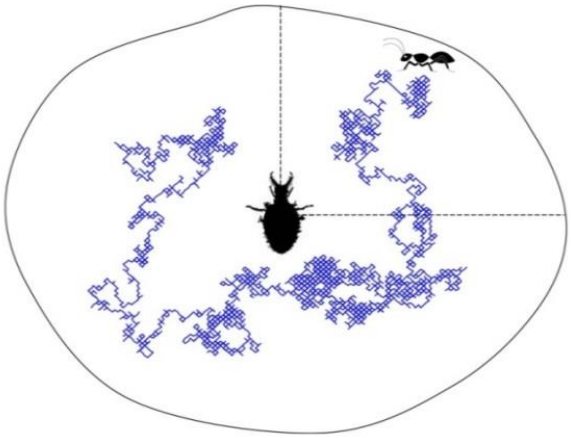

Fig. 3 – Random walk of an ant inside an antlion trap by Mirjalili [5].

Furthermore, ant lion discharges sand out of the pit center when upon realizing a trapped ant. This leads the trapped ant, which is trying to get away, to slip down. In order to design a model for such action, the ants' random walks hyper-sphere radius is reduced accordingly. This step is named sliding ants against toward antlion. Eq. (16) is suggested by Mirjalili [7] for this purpose

$$c^t = \frac{c^t}{I}, \quad d^t = \frac{d^t}{I}, \tag{16}$$

where I is a ratio calculated as Eq. (17):

$$I = 10^w \cdot \frac{t}{T}. \tag{17}$$

Such that t is the present iteration, T is the maximal iterations number, w is the constant dependent on present iteration as Eq. (18):

$$w = \begin{cases} 2 & \text{if} \quad t > 0.1T \\ 3 & \text{if} \quad t > 0.5T \\ 4 & \text{if} \quad t > 0.75T \\ 5 & \text{if} \quad t > 0.9T \\ 6 & \text{if} \quad t > 0.95T. \end{cases} \tag{18}$$

In fifth step, the hunting of ants by the predator and subsequently reconstructing the pit to hunt more ants is denoted by the equations below [7]:

$$Antlion_j^t = Ant_i^t \quad \text{if} \quad f(Ant_i^t) > f \tag{19}$$

Such that t exhibits the present iteration, $Antlion$ refers the location of chosen j^{th} ant lion at t^{th} iteration, and Ant_i^t illustrates the location of i^{th} ant at t^{th} iteration. The last step is elitism. It is presumed that every ant walks randomly at the vicinity of a selected ant lion by the roulette wheel (R_A^t) and the elite concurrently (R_E^t) at t^{th} iteration as Eq. (20):

$$Ant_i^t = \frac{R_A^t + R_E^t}{2}, \tag{20}$$

where Ant_i^t represents the location of i-th ant at t-th iteration.

5. VALIDATION OF THE RESULTS

For the purpose of verifying the ALO results, two common algorithms were selected i.e. Particle Swarm Optimization (PSO) as the most optimal algorithm from swarm-based techniques and Genetic Algorithm (GA) as the most optimal evolutionary algorithm. Effective parameters of ALO, GA and PSO algorithm are listed in Table 1.

Table 1

The values of effective parameters for each algorithm

GA	PSO	ALO
Population size = 30 Maximum of iteration = 120 Probability of crossover (Pc) = 0.8 Probability of mutation (Pm) = 0.03 ncrossover = 2*round(npop*Pc/2) nmut = npop*Pm	Population size = 30 Maximum of iteration = 120 Cognitive component = $c_1 = 2.05$ Social component = $c_2 = 2.05$ $w = \dfrac{0.1}{\left\lvert 1 - \dfrac{c}{2} - \dfrac{\sqrt{\lvert c^2 - 4c \rvert}}{2} \right\rvert}$, $c = c_1 + c_2$	Population size = 30 Maximum of iteration = 120 Random values= [0,1]

For the purpose of accumulating quantitative outcomes, every algorithm is performed on test functions more times and also to derive the mean and standard deviation of top rounded solution for the final iteration. Table 2 shows the outcome of the mean and standard deviation for the optimal stress around quasi-square hole for ALO, PSO and genetic algorithms.

Table 2

Statistical results of the algorithms on the aim functions

Aim Function	ALO		GA		PSO	
	Ave	Std	Ave	Std	Ave	Std
$w=0$	1.6924	0.1267	1.6965	0.1273	1.6955	0.1280
$w=0.05$	1.5558	0.0958	1.5585	0.0979	1.5568	0.0969
$w=0.1$	1.7484	0.0542	1.7512	0.0551	1.7501	0.0543
$w=0.15$	2.2133	0.1361	2.2164	0.1366	2.2101	0.1396
$w=0.2$	3.082	0.266	3.111	0.267	3.111	0.267

It is evident that the mean value of optimal stress achieved by the ALO is less compared to the other algorithms. Moreover, the ALO standard deviation is closer to zero in comparison to the PSO and GA algorithms. Therefore, it is deduced that the ALO exhibits superior performance compared to the other algorithms. Because of the stochastic characteristic of the algorithms, there was a need to conduct a statistical test to determine the significance of the results. The standard deviation and averages only compared the overall algorithms performances whilst a statistical test takes the results of every run into consideration and validates the statistical significance of the results. The Wilcoxon nonparametric statistical test was also implemented in this study. Here, $\alpha<0.1$ is assumed. The Wilcoxon test was applied for two hypotheses. The null hypothesis denotes the performance quality of all three optimization algorithms $\left(H_0 : \chi_1 = \chi_2 = \chi_3\right)$, and the other hypothesis addresses the absence of quality concerning the optimization algorithms and proves the advantages of the ALO in comparison to the PSO and genetic algorithms $\left(H_1 : \chi_1 \neq \chi_2 \neq \chi_3\right)$. Based on the results obtained from the Wilcoxon test, the P values acquired from this approach between the ALO and GA is 0.047. In addition, the P values between the ALO and PSO are equal to 0.068. The obtained P values denote such superiority is statistically profound because the values of P are

smaller than 0.1. Thus, the null hypothesis is dismissed regarding both comparative examples. This is an advantage of the ALO adequacy to obtain optimal stress surrounding the quasi-square hole. It can be deduced that the ALO algorithm takes advantage of great exploitation. Such great exploitation aids the ALO algorithm to promptly reach the global optimal state whilst achieving accurate exploitation. Constraints possess lower and upper boundaries that can be varied on the basis of the hole's shape. Eq. (21) presents the range of constraints for the quasi-square hole.

$$0 < \gamma < 90;\ \ 0 < \beta < 90;\ \ 0 < \omega < 0.33. \tag{21}$$

According to Eq. (21), the design variables are hole orientation (β), fiber angle (γ) and the curvature of hole corner (ω).

6. RESULTS AND DISCUSSION

Many parameters affect the stress distribution around a quasi-square hole within composite plates. For all results, the normalized stress is determined as $\sigma_{norm} = \dfrac{\sigma_\theta|_{\max}}{E_{11}\alpha_{11}q/k_{11}}$, where $\sigma_\theta|_{\max}$ is the maximum circumferential stress induced at the hole vicinity. The mechanical properties of materials used in this research are provided in Table 3.

Table 3

Materials properties of perforated plate [11]

Material	E_{11} (GPa)	E_{22} (GPa)	G_{12} (GPa)	υ_{12}	α_{11} (K^{-1})	α_{22} (K^{-1})	K_{11} ($Wm^{-1}K^{-1}$)	K_{22} ($Wm^{-1}K^{-1}$)
E-glass/Epoxy Wet	35	9	4.7	0.28	5.5×10^{-6}	2.5×10^{-5}	2.2	1.1
Epoxy Carbon Woven	91.82	91.82	19.5	0.05	2.5×10^{-6}	2.5×10^{-6}	3.5	2.6
Epoxy Carbon Woven Wet	59.16	59.16	17.5	0.04	2.2×10^{-6}	2.2×10^{-6}	0.81	1.059
Epoxy Carbon UD	200	9.45	5.5	0.27	0.4×10^{-6}	30×10^{-6}	0.7	1.21
$E_{33}=E_{22},\ G_{12}=G_{13}=G_{23},\ \upsilon_{12}=\upsilon_{13}=\upsilon_{23},\ \alpha_{33}=\alpha_{22},\ K_{33}=K_{22},\ K_{12}=0$								

6.1. Effect of fiber angle

The effect of fiber angles on the composite perforated plate on minimal thermal stress around a quasi-square hole is presented in Table 4. In this table, hole aspect ratio of size is 1 ($c=1$) and flux angle of 270 degrees ($\delta=270°$) is considered. The bluntness and rotation angle values are the optimal values achieved by the ALO algorithm. Based on Table 4, when the fiber angle is 90°, the maximum cost function value is obtained for all the materials whilst the carbon/epoxy UD material exhibits the highest stress compared to the other three materials. Furthermore, when the fiber angle is 45° for the carbon/epoxy woven wet, carbon/epoxy woven and glass/epoxy wet materials, the minimum cost function is achieved.

Table 4

Optimal values of different parameters for quasi-square hole in various fiber angles

Glass/epoxy wet				Carbon/epoxy woven			
γ	β	ω	C.F.	γ	β	ω	C.F.
0	45.0086	0.0456	1.5336	0	45	0.060708	1.083
30	48.8893	0.03155	1.452	30	66.0365	0.054764	0.92836
45	36.0966	0.034053	1.4325	45	0	0.0179	0.85296
60	34.9063	0.06056	1.5484	60	23.9464	0.05452	0.92825
90	44.995	0.071192	1.7003	90	45	0.0602795	1.0832

Table 4 (continued)

Carbon/epoxy woven wet				Carbon/epoxy UD			
γ	β	ω	C.F.	γ	β	ω	C.F.
0	45	0.03706	0.73865	0	90	0.04733	1.6055
30	69.3777	0.03663	0.69735	30	0	0.06736	1.9393
45	90	0.02067	0.68424	45	11.3103	0.0783073	2.0744
60	20.5278	0.0362011	0.69731	60	21.2333	0.0706858	2.1905
90	44.9998	0.036623	0.73864	90	45.0099	0.0652349	2.2656

6.2. Effect of rotation of the hole

By considering the flux angle of 270° and aspect ratio of hole size ($c=1$) the effect of the hole rotation angle on the minimum thermal stress around a quasi-square hole is presented in Table 5. Based on this table, the minimum cost function occurs at angles of 0° and 90° for three last materials and minimum cost function is at angles 45° for glass/epoxy wet material. In this part, carbon/epoxy UD material exhibits the highest thermal stress (equal to 1.7163) amongst the four others material and carbon/epoxy woven wet material exhibits the lowest value of thermal stress in situation of $\omega=0.02059$ and $\gamma=45$ degrees is equal to 0.68425.

Table 5

Optimal values of different parameters for quasi square hole in various rotation angles

Glass/epoxy wet				Carbon/epoxy woven			
β	γ	ω	C.F.	β	γ	ω	C.F.
0	38.9601	0	1.5104	0	45.0018	0.01651	0.85301
30	43.7106	0.0191	1.4836	30	44.9956	0	0.86583
45	35.5002	0.02753	1.4276	45	44.9995	0	0.86577
60	35.6777	0.010457	1.5019	60	44.5723	0.0032	0.86822
90	38.39589	0	1.5104	90	44.9995	0.01692	0.85299
Carbon/epoxy woven wet				Carbon/epoxy UD			
β	γ	ω	C.F.	β	γ	ω	C.F.
0	44.9944	0.0196712	0.68429	0	0	0.04731	1.6055
30	45.0176	0.00016	0.70506	30	0	0	1.7163
45	44.9929	0.00012	0.70507	45	0	0	1.7163
60	44.9752	0.0001	0.70492	60	0	0	1.7163
90	45	0.02058	0.68425	90	0	0.04731	1.6055

6.3. Effect of bluntness of the hole

The bluntness parameter (ω) is a prominent factor that influences the thermal stress distribution around the hole. For the purpose of assessing the impact of this factor, the optimal values of rotation angle (β) and fiber angle (γ) subjected to constant heat flux in status of $\delta=270°$ and $c=1$ for composite perforated plate are presented in Table 6 for different values of ω. the optimum amount of stress obtains in $\omega=0.05$ for glass/epoxy wet, carbon/epoxy woven, carbon/epoxy woven wet and carbon/epoxy UD are equal to 1.4682, 0.8642, 0.70479 and 1.6055 respectively. Based on this table, the minimum normalized stress value is significantly reliant on the value of ω.

Table 7 presents the overall optimal outcomes for the different composite materials. Here, design variables include fiber angle (γ), rotation angle (β) and bluntness (ω). In this table the normalized stress related to circular hole is denoted by $\bar{\sigma}_c$ and the table's last column denotes the percentage variance among the optimal stress value and $\bar{\sigma}_c$. Based on the results presented in Table 7, by selecting the optimum values of aforementioned parameters the value of the cost function can be decreased 5.8% for glass/epoxy wet, 1.5% for carbon/epoxy woven, 4.6% for carbon/epoxy woven wet and 6.9% for carbon/epoxy UD as

compared to a circular hole. Also, the results show that a circular hole ($\omega = 0$) is not always an optimum shape of hole.

Table 6

Optimal values of different parameters for quasi square hole for different ω

Glass/epoxy wet				Carbon/epoxy woven			
ω	γ	β	C.F.	ω	γ	β	C.F.
0	38.9447	0.01954	1.5104	0	44.9969	29.7863	0.8657
0.05	31.4397	48.5942	1.4682	0.05	53.3002	19.7573	0.8642
0.1	62.109	37.4879	1.6682	0.1	56.0795	22.2926	1.0035
0.15	72.2733	40.2343	2.03	0.15	56.0778	21.6929	1.2697
0.2	80.8634	42.9367	2.7161	0.2	55.3218	20.2568	1.7512
Carbon/epoxy woven wet				Carbon/epoxy UD			
ω	γ	β	C.F.	ω	γ	β	C.F.
0	44.997	11.6441	0.71572	0	0	67.5003	1.7162
0.05	29.6227	67.113	0.70479	0.05	0	0	1.6055
0.1	26.4331	63.0922	0.86823	0.1	60.3291	21.948	2.2657
0.15	62.5041	26.816	1.1169	0.15	82.5442	39.3732	2.8496
0.2	60.8033	26.2812	1.5553	0.2	86.8897	37.5172	4.0903

Table 7

Overall optimum results of square hole

Material	γ	β	ω	Optimum normalized stress	$\bar{\sigma}_c$	Percent reduction
Glass/epoxy wet	34.0675	46.307	0.02683	1.4276	1.5104	5.8%
Carbon/epoxy woven	45.4404	2.1017	0.01764	0.853	0.8657	1.5%
Carbon/epoxy woven wet	0.001	0	0.04731	0.6842	0.7157	4.6%
Carbon/epoxy UD	46.2192	23.69	0.02006	1.6055	1.7162	6.9%

7. CONCLUSIONS

In this study, ALO algorithm was implemented to determine the optimal values of parameters that affect the normalized stress around a quasi-square hole in composite plates. The hole rotation angle, bluntness and fiber angle have a substantial impact on the distribution of optimal thermal stress were considered as design variables. Different algorithms such as PSO, GA and ALO were employed to assess the ability and actions of the ALO to derive optimum values of the effective parameter. By applying the complex variable method, the thermal stress distribution around the quasi-square hole in composite plates was calculated. Results indicated that hole bluntness is not the sole factor influencing stress concentration reduction. The hole orientation and suitable fiber angle are also influencing factors in reducing thermal stress. The selection of optimal values for such parameters in particular curvatures entail significant reduction of stress concentration. The optimum values of normalized stress for quasi-square hole were more efficient than the circular hole.

REFERENCES

1. M. JAFARI, M.B. NAZARI, A. TAHERINASAB, *Thermal stress analysis in metallic plates with a non-circular hole subjected to uniform heat flux*, European Journal of Mechanics – A/Solids, **59**, pp. 356-363, 2016.
2. P. VIDAL, L. GALLIMARD, O. POLIT, *Modeling of composite plates with an arbitrary hole location using the variable separation method*, Computers and Structures, **192**, pp. 157-170, 2017.
3. H. PENG , Y. LIU, H. CHEN, J. SHEN, *Shakedown analysis of engineering structures under multiple variable mechanical and thermal loads using the stress compensation method*, International Journal of Mechanical Sciences, **140**, pp. 361-375, 2018.

4. A. KAMI, B. MOLLAEI DARIANI, A. SADOUGH VANINI, D-S. COMSA, D. BANABIC, *Application of a GTN damage model to predict the fracture of metallic sheets subjected to deep-drawing*, Proc. Ro. Acad., Series A, **15**, *3*, pp. 217-314, 2014.
5. M. JAFARI, M. JAFARI, *Thermal stress analysis of orthotropic plate containing a rectangular hole using complex variable method*, European Journal of Mechanics – A/Solids, **73**, pp. 212-223, 2019.
6. P. PANDEY, S. KUMAR, S. DAS, E.-M. CRACIUN, *Numerical solution of two dimensional reaction-diffusion equation using operational matrix method based on Genocchi polynomial. Part I: Genocchi polynomial and opperational matrix*, Proc. Ro. Acad., Series A, **20**, *4*, pp. 393-399, 2019.
7. S. MIRJALILI, *The Ant Lion Optimizer*, Advances in Engineering Software, **83**, pp. 80-98, 2015.
8. H. CAI, A. LU, Y. MA, *Shape optimization of two interacting holes with different areas in an infinite plate*, European Journal of Mechanics – A/Solids, **55**, pp. 78-89, 2019.
9. M. JAFARI, M.H. BAYATI CHALESHTARI, *Using dragonfly algorithm for optimization of orthotropic infinite plates with a quasi-triangular cut-out*, European Journal of Mechanics – A/Solids, **66**, pp. 1-14, 2017,
10. M. JAFARI, M. JAFARI, *Effect of uniform heat flux on stress distribution around a triangular hole in anisotropic infinite plates*, Journal of Thermal Stresses, **41**, pp. 726-747, 2018.

Received September 5, 2019